Multivariate random forest prediction of poverty and malnutrition prevalence

Chris Browne[1*], David S. Matteson[2†], Linden McBride[3†], Leiqiu Hu[4‡], Yanyan Liu[5‡], Ying Sun[6‡], Jiaming Wen[6‡], Christopher B. Barrett[7†],

1 Center for Applied Mathematics, Cornell University, Ithaca, NY, USA
2 Department of Statistics & Data Science, Cornell University, Ithaca, NY, USA
3 Department of Economics, St. Mary's College of Maryland, St. Mary's City, MD, USA
4 Department of Atmospheric and Earth Science, University of Alabama in Huntsville, Huntsville, AL, USA
5 Markets, Trade and Institutions Division, International Food Policy research Institute, Washington, DC, USA
6 School of Integrative Plant Science, Soil and Crop Sciences Section, Cornell University, Ithaca, NY, United States
7 Charles H. Dyson School of Applied Economics and Management, Cornell University, Ithaca, NY, USA

† These authors contributed equally to this work.
‡These authors also contributed equally to this work.
* cnb49@cornell.edu

Abstract

Advances in remote sensing and machine learning increasingly enable estimation of tolerably accurate, inexpensive, and timely indicators of poverty and malnutrition status to guide development and humanitarian agencies' programming. However, state of the art models often rely on proprietary data and/or complex algorithms. We demonstrate how a relatively simple statistical model can produce estimates of a set of (potentially correlated) malnutrition and poverty prevalence measures using free, open access, regularly updated, georeferenced data. We demonstrate two use cases: contemporaneous prediction which might be used for poverty mapping and geographic targeting, and sequential prediction that can inform early warning systems. Applied to data from 11 low and lower-middle income countries, we find comparable predictive accuracy in both tasks to estimates from more sophisticated methods and data.

1 Introduction

Governments and humanitarian agencies devote considerable resources towards poverty and malnutrition reduction efforts. One key factor in the effectiveness of such efforts is the accuracy with which poor and malnourished populations can be identified. The more quickly and accurately these subpopulations can be targeted for intervention, the lower the likelihood that adverse agricultural, economic, political, or weather shocks will thrust these vulnerable groups into poverty traps or famine [1, 2].

To inform aid targeting efforts, agencies have historically drawn data mainly from detailed household surveys, such as the large-scale, nationally-representative Demographic and Healthy Surveys (DHS) or Living Standards Measurement Study (LSMS) programs. Such surveys are, however, expensive and time-consuming, and may systematically omit subregions that are harder or more dangerous to physically access, despite the severe poverty and malnutrition prevalence likely endemic to such locations. Moreover, high-quality, large-scale surveys are typically fielded only once every several years, and are generally statistically representative of the population only at relatively large (e.g. provincial or regional) scales under standard sampling protocols. Although higher frequency surveys can improve the timeliness of survey coverage, this often comes at the cost of spatial and survey detail [3]. While certainly useful, the shortcomings of these survey-based estimation techniques for up to date or forward looking poverty and malnutrition prevalence can ultimately hinder the development of timely and effective humanitarian programming, especially in circumstances where rapid response is needed.

Recent advances in remote sensing (RS) and machine learning (ML) offer tantalizing prospects to resolve some of these shortcomings by providing accurate, cheap, and timely indicators of poverty and malnutrition status, at high spatio-temporal resolution, and the means to transmit these data into actionable predictions for policy. Most of the recent literature applying statistical and ML methods to predict poverty and malnutrition status focus on the contemporaneous prediction case, which bears important similarities to the well-established poverty mapping literature, which is in turn based on small area estimation methods [4–6].

More recently, Jean *et al.* [7] pioneered the use of deep learning methods, and in particular convolutional neural networks trained in conjunction with transfer learning methods and RS data, to identify nationwide poverty incidence at high spatial resolution (i.e., village or county level). Their innovations promise much lower data costs and more current estimates than conventional poverty mapping methods that

rely on household surveys and census data alone. The past few years have brought many useful refinements of these methods, alongside variations in precise statistical methodology and target outcome [8–17].

Although famine early warning systems have over the last decade made heavy use of RS data measuring weather patterns, vegetation health, and food prices, many of the features we use here, as key information sources [18, 19], there has been less use of statistical methods to forecast future poverty or malnutrition status in the absence of intervention based on this information, despite their potential value to the humanitarian response community. In spite of the the challenges inherent to poverty and malnutrition forecasting, some analysts have demonstrated some context-specific success. For example, Mude *et al.* [20] used several years of monthly observations at the community level (roughly equivalent to DHS surveys clusters) to predict children's mid-upper arm circumference in northern Kenya using multivariate regression methods, while Yeh *et al.* [12] and Tang *et al.* [21], apply deep learning methods to predict temporal changes in household poverty measures.

Ongoing challenges in this fast-moving field include the development of rigorous methods that can produce tolerably accurate and timely predictions of poverty and malnutrition status using open access and near-real time data, to assess how the quality of these predictions change when moving between contemporaneous prediction and forecasting, and to identify the types of RS data which are most valuable for such predictions. Furthermore, as such methods must be easily employable by operational agencies at feasible cost and effort, it remains important to assess whether the use of more sophisticated predictive methodologies produces gains in predictive performance large enough to justify their more expensive and technically demanding application.

This paper engages with these challenges by demonstrating how free, open access, regularly updated, georeferenced data can be analyzed using a relatively simple statistical model to provide estimates of a set of malnutrition and poverty indicators, with accuracy comparable or superior to estimates based on more complicated algorithms. We demonstrate this for two use cases: a) contemporaneous mapping of poverty and malnutrition indicators, i.e., contemporaneously predicting prevalence at both surveyed and unsurveyed locations within a given country and survey year, and b) early warning, or forecasting future prevalence levels based on historical observations. Consistent with prior findings, we find it is much easier to predict the prevalence of asset poverty than of child malnutrition indicators [9], and find forecasting to be more challenging than contemporaneous prediction [12]. Because poverty and malnutrition indicators are typically correlated, we also examine whether multivariate methods, which predict several indicators simultaneously, could enhance poverty and malnutrition prediction, and find mixed results. In some but not all cases, the accuracy of predictions of multiple indicators modestly exceeds that of predicting each independently.

In explaining poverty and malnutrition prevalence, we find that geographic variables that are unlikely to change much over just a few years have the greatest explanatory power, followed by vegetation and climate data. Although conflict and food price shocks elicit considerable attention, we find they contribute relatively little to the prediction of malnutrition and poverty indicators. As a final contribution, we also provide our full set of training and testing data in the hopes that its availability might further global efforts in poverty and malnutrition prediction.

2 Data description

We focus on data from eleven USAID Feed the Future (FTF) priority countries: Bangladesh, Ethiopia, Ghana, Guatemala, Honduras, Kenya, Mali, Nepal, Nigeria, Senegal, and Uganda. We restrict ourselves to publicly available data so as to represent what might be feasible for agencies unable to invest scarce resources in data collection or procurement. We describe the data sources in this section before discussing data pre-processing in the next section. Though publicly available data has become increasingly plentiful, curation of standardized, spatially and temporally matched, regularly updated data remains an undersupplied public good.

2.1 DHS malnutrition and asset poverty data

Our key poverty and malnutrition outcome indicators all come from ARENA aggregated DHS survey data or directly from the DHS; with the sample size, country, and dates of these surveys detailed in Table S5. We extract from these surveys cluster or enumeration area (EA) level prevalence estimates of these five outcomes, each of which were weighted by household survey sampling weights (with the exception of the data on women's underweight BMI, which was weighted with individual survey sampling weights):

1. Asset poverty: households in the poorest quintile of the asset-based comparative wealth index, defined as an asset index score $\leq$ -0.9080 (FTF 2018);
2. Child stunting: children under five years of age whose height-for-age z-score is $<$ -3.0 standard deviations below the median on the World Health Organization (WHO) Child Growth Standards;
3. Child wasting: children under five years of age whose weight-for-height is $<$ -2.0 standard deviations below the median on the WHO Child Growth Standards;
4. Healthy weight: children under five years of age whose weight-for-height falls in the interval [-2.0,2.0] standard deviations from the median on the WHO Child Growth Standards;
5. Underweight women: those ages 15 to 49 whose body mass index (BMI) $<$ 18.5.

While the first four indicators were compiled from raw DHS data by ARENA, and briefly verified by us through comparison to DHS summary statistics, we estimated the women's underweight prevalence series independently from DHS surveys. These indicators serve as our dependent variables, and in the following subsections, we detail a suite of input features (covariates) used for prediction of these quantities. In addition to these prevalence rates, we also extract from DHS the physical location (latitude and longitude) of each EA, which allow for georeferencing of other inputs to enumeration locales. We also include the date of a given survey as a feature, capturing the possibility of year-specific shocks common to all DHS clusters in a given survey round, and include an indicator variable on whether the cluster is urban or rural.

2.2 Physical geography covariates

Our first set of covariates describe the physical geography of locations, and were extracted from the ARENA data series compilation:

- Travel time to the nearest city with a population of 500,000 or more persons, as derived from IFPRI's modeled estimates of market accessibility surface globally

as the travel time from household locations to the nearest city, as described in [22–24].

- Percent tree cover data produced by [25] and presented at 1 km spatial resolution;
- Pasture coverage data present at 5 minute (∼10 km) spatial resolution drawn from Ramankutty et al's [26] data series on agricultural lands in 2000;
- Altitude measured as the pixel elevation in meters above/below sea level; the data are drawn from Shuttle Radar Topography Mission data made available by the NASA Jet Propulsion Laboratory and the California Institute of Technology
- Slope, calculated by the IFPRI ARENA team as the degree gradient of steepness.

These features are then associated with DHS enumeration areas by matching to each EA the feature values that are physically closest to it in space, and are assumed constant for the duration of our analysis.

2.3 Food price data

As demonstrated by global food price spikes during the 2007-12 period vividly demonstrated, food prices can affect poverty and malnutrition patterns over space and time, as high food prices hurt poor urban residents and rural net food consumers who tend to be smallholders or landless [27]. Open access food price data may therefore be useful for monitoring changes in poverty and malnutrition patterns in a timely manner.

We collect food price data from the Food and Agriculture Organization (FAO) Food Price Monitoring and Analysis site, which provides monthly market-level data for major food commodities in most countries. Table S6 summarizes these data by the number of food types monitored, number of geographic markets included, whether the data reflect retail or wholesale prices, and the first available observations in the time series, for each country. Noting that both the value and volatility of food prices can impact poverty and malnutrition prevalence, we associate with each DHS enumeration area as features both the mean and variance of each food commodity price recorded by FAO within that survey's country, measured in USD per kg (with the exception of Bangladesh, where prices are reported per ton). Food price means and variances are computed over a one-year window prior to the beginning of each DHS survey, with market locations georeferenced to the centroid of that market's resident city, and with incomplete records excluded from analysis. Food price features are then assigned to EAs in a spatially ordered fashion, with the n-th set of food price features coinciding with those food price features extracted from the n-th nearest market to the EA.

2.4 Solar-induced chlorophyll fluorescence data

The quality and abundance of locally produced crops can have a direct impact on the poverty and malnutrition status of households. Solar-induced chlorophyll fluorescence (SIF) is an optical signal emanating from the core of plants' photosynthetic machinery, which contains more direct functional information about photosynthesis [28], and is less sensitive to atmospheric contamination than many conventional greenness measures [29], making SIF an ideal measure of crop yield and health, as evidenced by its efficacy in yield prediction for both US Corn Belt and Australian wheat production [30–32]. The recent advent of satellite based RS methods for SIF measurement [33–37] allows us to easily incorporate vegetative health into our model, and we use in particular a new, long-term, high-resolution, SIF time series developed

by Wen *et al.* [38]. This time series is recorded at monthly, 0.05 degree resolution, and uses data fusion techniques to both downscale and merge SIF retrievals from the Scanning Imaging Absorption Spectrometer for Atmospheric Chartography (SCIAMACHY) and the Global Ozone Monitoring Experiment-2 (GOME-2) [39] to construct a long-term, high resolution, dataset, from 2003 to 2018, which has been independently validated with both ground and airborne measurements.

Given the pronounced seasonality typical to agricultural production, alongside populations' adaptations to these seasonal patterns, we assume that deviations from seasonally typical (mean) SIF conditions will serve as a better indicator of imminent food and poverty crises than will raw values. From raw SIF readings, we thus construct a set of four z-scores. These four z-scores each correspond to one of of four non-overlapping, three month, periods, roughly approximating seasons. Z-scores for a given location and season are computed using the sample mean and sample standard deviation of all raw SIF values observed during that season, and which are within 100 km of the target location. For each EA, we then assign as feature the mean of the four seasonal z-scores generated from the four seasons immediately prior to survey start date, and whose sensing location is closest to the enumeration area in space.

2.5 Land surface temperature data

Land surface temperatures (LST) are often estimated from satellites for purposes of drought and vegetation stress monitoring in agricultural systems [40]. Spatiotemporal variation in LST can reflect the variation in the physical processes of land-atmosphere interactions, which can in turn affect both plant evapotranspiration and surface moisture [41]. Historical satellite derived LST products have relatively coarse spatial resolutions, e.g., 0.05 degrees or worse, and suffer from spatiotemporal bias and inconsistencies when assessed at monthly scale due to the appearance of clouds and infrequent observation [42, 43].

We therefore use the new, longer-term, and higher-resolution, LST series, MYD11A1 (daytime), constructed from the Afternoon Satellite Aqua overpass. This series contains monthly composites of daily LST observations, at 1km resolution, between 2003-18 [44]. To ensure sufficient coverage, satellite pathing is controlled to ensure observation times are close to the time of daily maximum LST, while missing or anomalous readings caused by clouding are imputed using a physics-based, diurnal, temperature cycle model, which is evidently effective [45–47].

As recent studies suggest that maximum temperature is a more useful predictor of surface droughts, and thus shocks to poverty and malnutrition prevalence, than mean temperature at both annual and monthly scales [44, 48], we extract from this series in particular monthly composites of daily maximum LST for use in modeling. Again assuming that deviations in maximum monthly LST will be more indicative of poverty and malnutrition status due to population adaptation to typical temperatures, we again apply the same seasonal normalization procedure used for SIF data assignment, and again assign to each EA the mean of the four maximum LST z-scores generated during the four seasons immediately prior to survey start date, and which are sensed closest to the EA in space.

2.6 Precipitation data

As precipitation and rainfall are intimately linked to both crop production and water availability, we use monthly, 0.05 degree, precipitation data from the Climate Hazards

group Infrared Precipitation with Stations (CHIRPS) as a metric for water availability [49]. CHIRPS data is produced based on satellite and station observations, together with precipitation climatology informed imputation, as described in [50]. These data have been widely validated and employed to characterize water availability and detect drought, especially on the African continent [50–55]. We again use as features seasonally normalized readings, and again assign to each EA the mean of the four CHIRPS derived z-scores generated during the four seasons immediately prior to the survey start date that are sensed closest to the EA in space.

2.7 Conflict data

Armed conflict and political instability are well known to cause adverse shocks in food security and poverty status [56]. To incorporate these phenomena, we source data from the Uppsala Conflict Data Program (UCDP) [57, 58] which provides descriptions of violent events, or incidents wherein "armed force was used by an organized actor against another organized actor, or against civilians, resulting in at least 1 direct death at a specific location and a specific date". To adhere to this definition, UCDP data include violent events only if there are clear estimates of fatalities and a clear indication of actors involved.

In preprocessing, we remove events that lack a georeference (roughly 10 percent of events), or timestamp (roughly 3 percent). Because violent conflict commonly represents country-level political instability and because the conflict data are relatively sparse, we treat the conflict data in a country-specific but otherwise spatially agnostic framework, and associate with each given survey in a particular country the number of violent events and number of resulting casualties occurring in the year prior to the DHS survey start date. As many violent events are part of a more protracted conflict, these counts also include all longer (greater than 1 day) events whose terminal date lies within the one-year window prior to the start date of each DHS survey.

2.8 Additional preprocessing

As a final stage of preprocessing, we remove any features that are missing for more than 20 percent of a given test/train regime (soon to be discussed), and remove datums that contain any additional missing features or outcomes. Due to occasional variation in the exact commodity prices reported by FAO within each country across survey years, this former decision causes the occasional omission of market price data when analyzing certain DHS surveys, while the latter results in omission of the 2012 and 2014 DHS surveys in Senegal, where underweight female BMI data are missing, alongside a small reduction in sample size.

3 Methodology

3.1 Modeling pipeline

To assess whether competitive predictions for poverty and malnutrition prevalence can be produced without the need for sophisticated deep learning models, we consider a simple random forest (RF) model. Random forests are among the most commonplace ML algorithms, and can be easily implemented using widely available off-the-shelf packages in many programming languages. We explore both independent RFs, which will predict each poverty or malnutrition outcome separately, as well as multivariate RFs, which employ joint estimation of outcomes.

As interventions targeting poverty and malnutrition prevalence are typically performed at country and year specific levels, and due to variation in both the number and meaning of food price features across countries, we assume a survey (i.e. country and year) specific relationship between model inputs and prevalence rates. For countries $c = 1, 2, ..., 11$, we denote by $(\mathbf{x}_i^{t,c}, \mathbf{y}_i^{t,c}) \in (\mathcal{R}^{p^c}, \mathcal{R}^5)$ respectively our p^c input features specific to country c and country agnostic outcomes (prevalences), with $i = 1, ...n^{t,c}$ counting the total number of EAs surveyed by DHS in country c during year t. Our survey specific model for joint prediction of the five target prevalence rates can then be written in a signal-plus-noise formulation:

$$\mathbf{y}_i^{t,c} = \mathbf{f}^{t,c}(\mathbf{x}_i^{t,c}) + \boldsymbol{\epsilon}_i^{t,c}, \tag{1}$$

where $\boldsymbol{\epsilon}_i^{t,c}$ are assumed i.i.d. across observations i for all years and countries, t and c, respectively, with mean $\mathbf{0}$, covariance $\Sigma^{t,c}$.

To allow for incorporation of possible dependencies between poverty and malnutrition prevalences, we model each mapping $\mathbf{f}^{t,c}$ via a (multivariate) Mahalanobis random forest (MRF) [59–61], which extends the traditional univariate random forest model to a multivariate setting in which joint prediction of outcomes is performed through the explicit inclusion of outcome dependencies that are estimated in training. Prediction within the context of an MRF is a straightforward extension of the traditional setting, with terminal nodes of a given tree containing as prediction the componentwise mean of resident outcome vectors, while forest predictions at a testing point $\mathbf{x}^{t,c}$ are analogously the componentwise average over the individual predictions $h_k^{t,c}(\mathbf{x}^{t,c})$ of each tree within the forest ensemble:

$$\begin{aligned} \hat{\mathbf{f}}^{t,c}(\mathbf{x}^{t,c}) &= \frac{1}{T}\sum_{k=1}^{T} h_k^{t,c}(\mathbf{x}^{t,c}), \\ h_k^{t,c}(\mathbf{x}^{t,c}) &= \frac{1}{|L_k(\mathbf{x}^{t,c})|}\sum_{i=1}^{n^{t,c}} \mathbf{x}_i^{t,c} \cdot I_{L_k(\mathbf{x}^{t,c})}(\mathbf{x}_i^{t,c}), \end{aligned} \tag{2}$$

where $L_k(\mathbf{x}^{t,c})$ denotes the leaf containing $\mathbf{x}^{t,c}$ in tree $k = 1 : T$, $|\cdot|$ denotes cardinality, and where $I_A(\cdot)$ is an indicator function on the set A, so $I_{L_k(\mathbf{x}^{t,c})}(\mathbf{x}_i^{t,c}) = 1$ if the ith input observation is in the same leaf as the testing point, and 0 otherwise.

The primary distinction of the MRF then comes in training, with node splits now chosen via Mahalanobis distance:

$$C_L(\mathbf{X}^{t,c}, \mathbf{Y}^{t,c}) = \sum_{i=1}^{n^{t,c}} (\mathbf{y}_i^{t,c} - \bar{\mathbf{y}}_L)' \Lambda^{t,c} (\mathbf{y}_i^{t,c} - \bar{\mathbf{y}}_L) \cdot I_L(\mathbf{x}_i^{t,c}), \tag{3}$$

where $\bar{\mathbf{y}}_L$ denotes the mean response vector within leaf L, and with $\Lambda^{t,c}$ denoting the precision matrix, i.e., the inverse of the covariance matrix $\Sigma^{t,c}$. The modified cost function (3) can then be reinterpreted as replacing the traditional variance criterion of random forest regressor with a sum of variances across independent output dimensions, following their decorrelation as specified by $\Lambda^{t,c}$. This allows for splits to be chosen in a way that jointly minimizes variance across outcomes while incorporating output dependency, ideally improving predictive performance by leveraging outcome dependencies.

3.2 Hyperparameter selection

We set $T = 2{,}000$ as our forest size, then chose random forest hyperparameters of max tree depth (d) and feature downsampling rate (dsr) via five-fold cross validation on training data. While this cross validation was initially performed separately for each survey, and separately for both sequential and contemporaneous frameworks, which will be discussed in the next section, we ultimately chose to select a single set of shared hyperparameters $d = 4, dsr = \frac{1}{3}$, corresponding to the modally selected hyperparameter values across all surveys and predictive frameworks, causing a negligible change in performance at the benefit of reproducibility and parsimony.

Since the error covariance matrices $\Sigma^{t,c}$ are in general unknown, we estimate them by first fitting a collection of univariate random forests for each country, year, and outcome, independently. Training residuals from these models were then used to directly estimate $\Sigma^{t,c}$, alongside its inverse $\Lambda^{t,c}$, for use in Equation 3, in an approach analogous to Feasible Generalized Least Squares. In testing, results from these independent random forest models are then used to establish a baseline against which to compare our joint model.

4 Results and analysis

We now consider two distinct predictive tasks. The first, which we term sequential prediction, is intended for use in early warning systems, and considers the forecasting of future poverty and malnutrition prevalence using historical data. The second, which we term contemporaneous prediction, is intended to inform geographic targeting in poverty or malnutrition interventions, or to be used for monitoring and evaluation purposes, and is used when one observes outcomes in only a sample of locations, which are to be generalized to a larger spatial domain based on these current survey year observations. Although these two tasks can use similar data and methods, we emphasize that these distinct use cases are not necessarily interchangeable, and we find considerable differences in predictive performance across these two regimes, underscoring the importance for agencies and analysts to define their intended task in modeling and evaluation.

4.1 Sequential prediction

To assess the ability of our model to forecast poverty and malnutrition prevalence, we consider a sequential prediction framework in which, for each country surveyed in year t, we predict poverty and malnutrition prevalence during this year using only historical data, drawn from previous DHS surveys in years $t' < t$ occurring in the same country. While minimally studied in the existing literature, we find that simple RFs, used in conjunction with open access data, can produce relatively accurate forecasts of certain prevalence rates, with modest improvements in forecast accuracy gained via our joint estimation approach, for certain prevalences.

We evaluate model performance for each indicator via out-of-sample r^2 and root mean squared error normalized (NRMSE) by (in-sample) observed prevalence range:

$$r_j^2 = 1 - \frac{\sum_{i=1}^{n}(y_{i,j} - \hat{y}_{i,j})^2}{\sum_{i=1}^{n}(y_{i,j} - \bar{y}_{i,j})^2}, \tag{4}$$

$$\text{NRMSE}_j = \frac{\sqrt{\frac{1}{n}\sum_{i=1}^{n}(y_{i,j} - \hat{y}_{i,j})^2}}{\max_{i=1:n}(y_{i,j}) - \min_{i=1:n}(y_{i,j})}, \tag{5}$$

where j denotes the jth prevalence $j = 1:5$ and where i denotes the ith EA area considered in a given test-train framework.

Predictive performance is assessed at three levels of aggregation. At the coarsest scale, we assess fully aggregate results, which are computed by pooling all predictions across all surveys, displayed in Table 1. We next assess predictive performance at the individual country level, wherein predictions are pooled across all surveys within each country, displayed in Fig 1, and with Table 2 reporting mean country level performance weighted by relative country survey size. Finally, at the finest level of aggregation, we report individual survey level performance, with results displayed at length in Appendix S1.

Table 1. Aggregate out-of-sample r^2 and NRMSE for sequential prediction, indexed by methodology and prevalence.

		Child Stunting	Child Wasting	Healthy Weight	Asset Poverty	Underwt Women
IRF	r^2	0.07	-0.01	-0.21	0.21	0.31
MRF	r^2	0.08	0.10	-0.04	0.21	0.29
IRF	NRMSE	0.21	0.15	0.16	0.26	0.17
MRF	NRMSE	0.21	0.12	0.15	0.27	0.12

Scores are computed by pooling all predictions across all surveys, with shared testing and training folds used across all models.

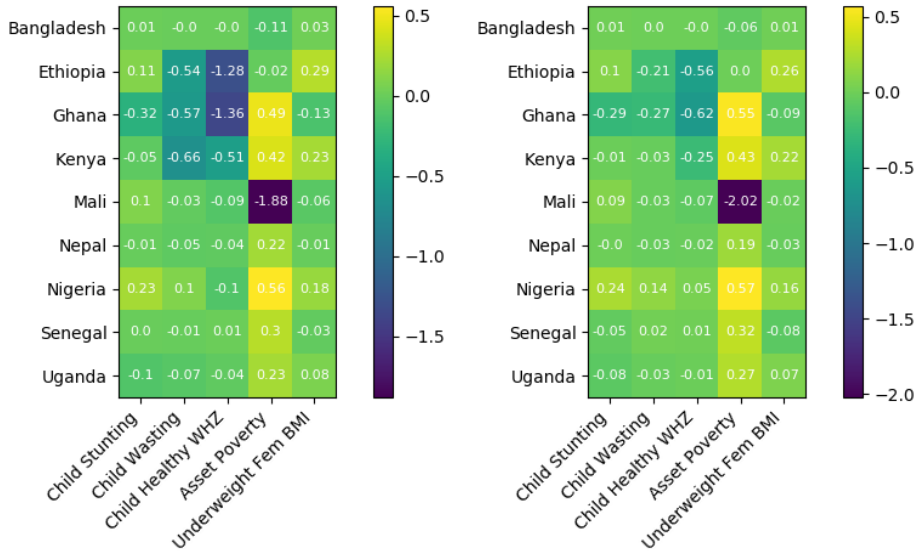

Fig 1. r^2 for sequential poverty and malnutrition prevalence prediction indexed by country. Left: Independent RF, Right: MRF. Scores are computed by pooling predictions across all surveys within each country, with shared testing and training folds used across all models.

Table 2. Mean country level out-of-sample r^2 and NRMSE for sequential prediction, indexed by methodology and prevalence.

		Child Stunting	Child Wasting	Healthy Weight	Asset Poverty	Underwt Women
IRF	r^2	0.01	-0.24	-0.39	0.12	0.11
MRF	r^2	0.02	-0.04	-0.17	0.13	0.10
IRF	NRMSE	0.21	0.16	0.17	0.24	0.17
MRF	NRMSE	0.21	0.14	0.16	0.24	0.17

Scores are computed by taking a size weighted average of individual country level performance, with shared testing and training folds used across all models.

As will be later shown, though forecasting of poverty and malnutrition prevalence appears to be a considerably more challenging task than contemporaneous prediction, we note decent performance in forecasting of asset poverty and underweight women prevalence, in comparison to our modest predictions for child stunting and wasting, while our least skilled predictions are of healthy weight children. Because healthy child weight is the complement of both child wasting and obesity, and because our predictions for child wasting are superior to our predictions for child healthy weight, this finding indicates that child obesity may be especially hard to predict with these data and methods. This hypothesis seems in line with theoretical foundations, as obesity appears strongly related to health insults in utero, lifestyle preferences, and cultural environment, none of which are readily captured by any of the data we use [62, 63].

Joint estimation of outcomes seems to produce modest improvements in forecasting of child nutritional outcomes, relative to independent RF modeling, as measured by r^2, due to the clear correlation between these indicators. We also note that for both independent random forest and MRF models, our relatively low NRMSEs indicate that these models can produce forecasts capable of reasonably informing aid planning and policy, being accurate to within roughly 10 to 25 percent of the observed range of each indicator, despite being generated 3-5 years in advance (see Table S5 for exact inter-survey times). We interpret these results as showing promise for the use of simple ML methods and open access data for early warning, and motivating joint estimation as a potential direction of future work.

As evident in Tables 1 and 2, and in Fig 1, we observe a considerable drop in performance, as measured by r^2, when assessing our results at more granular scales. This effect becomes more pronounced at the even finer survey level assessment scale, detailed in Appendix S1, where our model exhibits high variance in predictive performance on individual surveys, with a significant deterioration in mean performance. Considering these findings in the context of individual survey sizes listed in Table S5, we believe this drop in predictive performance at finer assessment scales arises largely from extremely poor performance on a subset of three outlier surveys, each of which is the first sequential testing year in countries with relatively small sample size DHS surveys. This hypothesis is further supported by directly comparing the impact of survey size on survey level predictive performance, displayed in Figure S6, and by noting our survey size weighted, mean, country-level performance remains well above the lower tail of individual country-level performance. In the context of our task, it should come as little surprise that attempting to forecast several years ahead from a small training set will generates inaccurate predictions. This shortcoming

should therefore diminish steadily as the history and/or sample size of DHS surveys grow, but, as will be later discussed, showcases a weakness of our model relative to competing methodologies based in transfer learning. An alternative explanation for these findings is that failure to incorporate spatial autocorrelation in our outcome variables might degrade predictive performance when moving from large scale analysis to finer spatial domains, where spatial associations exert stronger influence on outcome variability, resulting in worse relative fit [64]. Allowing for the possibility of spatial autocorrelation of outcomes therefore seems a fruitful direction of future work. Despite these findings, we note qualitatively similar NRMSE at both aggregate, country, and survey level scales (see Tables S1,S2). This suggests that our model can generate reasonably accurate predictions of key malnutrition and poverty indicators at different scales of analysis, even with relatively sparse data.

Despite our method's shortcomings, our results seem comparable to prior related works. While competing methods for sequential prediction of poverty and malnutrition prevalence are sparse, the most directly comparable work may be Yeh *et al.* [12], who predict changes in DHS asset poverty over time for a set of 23 sub-Saharan African countries using multispectral, convolutional neural networks. These authors report cluster level out-of-sample $r^2 = 0.18$, with minimal difference when predictions are assessed in aggregate or averaged over individual countries, as compared to our aggregate and country-level mean r^2s of 0.21 and 0.14, respectively. We emphasize that direct comparison of results is impossible due to differences in both the encoding of poverty status and the scope of analysis. Moreover, Yeh *et al.* [12] predict changes in poverty status, thus requiring access to future data for training, rather than forecasting poverty prevalence using only historical data, as we did.

Nevertheless, this comparison seems to establish a basic credence to our results, indicating that simple statistical methodologies can produce results competitive with those generated by considerably more sophisticated deep and or transfer learning based methods, when applied to the right data, even with infrequent observations. Given the relative ease of implementation of our MRF approach and the open access to our data, this seems a comparatively easy-to-implement, tolerably accurate, first pass method that agencies might use as part of a broader early warning system. Such preliminary findings could perhaps be usefully supplemented with proprietary data and more complex and costly transfer learning based approaches. We also note that although we had to exclude central American countries Guatemala and Honduras from our sequential prediction because they each had only a single year of georeferenced DHS data available, our work extends the sequential prediction of poverty and malnutrition prevalence beyond sub-Saharan Africa, to Bangladesh and Nepal, demonstrates that simple models of these phenomenon can be easily developed and applied globally with modest accuracy.

To demonstrate how the forecasts of our MRF model could be used to provide policymakers with visual, georeferenced, predictions of poverty and malnutrition prevalence, Fig 2 provides a visual depiction of a five-year ahead spatial forecast for asset poverty and child wasting prevalences across Nigeria, which was generated using 2008 DHS data and input features. Such maps are widely used in early warning systems because they provide effective visualization tools for policymakers, and inform the spatial allocation of scarce resources by logisticians [65]. When produced repeatedly over time, these maps can also be used to provide baseline, midline and endline measures for monitoring and evaluation purposes, and allow for estimation of poverty and malnutrition status in areas where reliable survey data may be

unavailable. We find these maps to show qualitative agreement with contemporaneous products developed by the Famine Early Warning System for Nigeria in 2013 [66], where the northwestern and northeastern regions exhibited the greatest concentrations of acute malnutrition and poverty, despite being produced 5 years in advance.

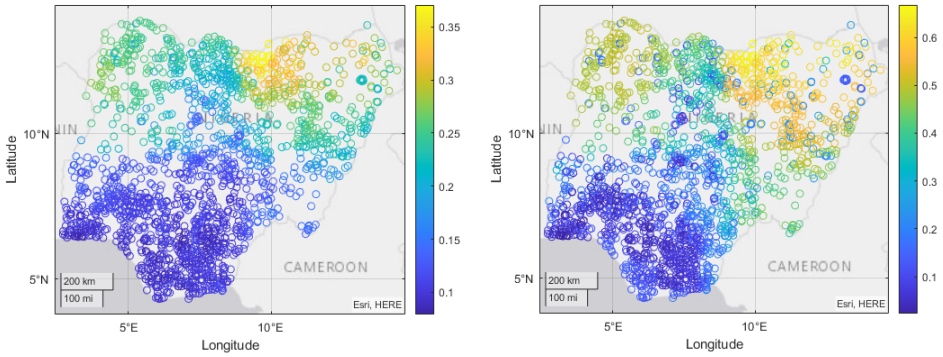

(a) Child Wasting **(b)** Asset Poverty

Fig 2. Five-year-ahead forecasts of child wasting and asset poverty prevalence for Nigeria, 2013.. Within survey r^2 are 0.10 and 0.56 for child wasting and asset poverty, respectively.

4.2 Contemporaneous prediction

A different, and typically easier, task is to use survey observations to predict contemporaneous values for unsurveyed locations. As discussed earlier, the resulting contemporaneous predictions can be very useful for monitoring and evaluation or geographic targeting purposes.

We next apply our MRF approach to a cumulative, contemporaneous, predictive task, wherein, for each country surveyed in year t, all data from previous survey rounds $t' < t$, along with 80 percent of the data from survey year t, are used for model training, with the remaining 20 percent of year t data held out for testing. Testing and training are performed five times for each survey, corresponding to five-fold cross validation across data from survey year t, with all results reported corresponding to the average score computed across all folds.

In Tables 3 and 4 we again assess our predictive results for contemporaneous prediction of poverty and malnutrition prevalence via our of sample r^2 and NRMSE. Again, predictions are assessed at three levels of granularity, with fully aggregate results displayed in Table 3, country-level and mean country-level results displayed in Fig 3 and Table 4, and with survey level results relegated to Appendix S1.

Table 3. Aggregate out-of-sample r^2 and NRMSE for contemporaneous prediction, indexed by methodology and indicator

		Child Stunting	Child Wasting	Healthy Weight	Asset Poverty	Underwt Women
IRF	r^2	0.28	0.23	0.17	0.58	0.48
MRF	r^2	0.27	0.23	0.17	0.58	0.46
IRF	NRMSE	0.19	0.11	0.14	0.19	0.11
MRF	NRMSE	0.19	0.11	0.14	0.19	0.11

Scores are computed using predictions across all countries and survey years and averaged over 5 folds. Testing and training folds are shared across models.

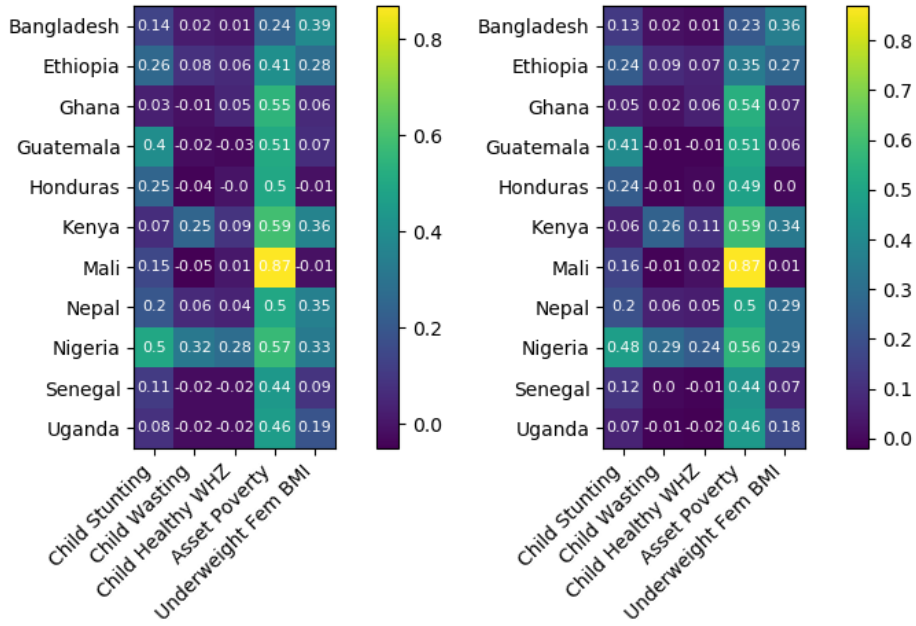

Fig 3. r^2 for contemporaneous poverty and malnutrition prevalence prediction by country. Left: Independent RF, Right: MRF

Table 4. Mean country level r^2 and NRMSE for contemporaneous prediction, indexed by methodology and indicator.

		Child Stunting	Child Wasting	Healthy Weight	Asset Poverty	Underwt Women
IRF	r^2	0.21	0.08	0.06	0.49	0.24
MRF	r^2	0.20	0.09	0.06	0.48	0.22
IRF	NRMSE	0.21	0.19	0.21	0.19	0.19
MRF	NRMSE	0.21	0.19	0.20	0.19	0.19

Scores are computed using predictions across all countries and survey years and averaged over 5 folds. Testing and training folds are shared across models.

Since contemporaneous prediction makes use of all the same features as the sequential prediction task, while having more current data, it should, and does, prove more accurate than sequential prediction. We find significant improvements in r^2 scores and more modest improvements in NRMSE relative to our sequential framework, for both independent and joint random forest models, and at all levels of aggregation. Unfortunately, and in contrast to the sequential prediction case, we find no performance improvement from joint estimation of malnutrition and poverty prevalence rates, indicating that the leverage gained through joint estimation of target outcomes may be less relevant when testing and training data are closer in time. Thankfully, we find that simple, univariate, random forest models can produce relatively accurate, and competitive, contemporaneous, predictions of both malnutrition and poverty prevalence rates. We again note a general reduction in performance when assessing model fit at a country and survey specific level, which presumably arises for the same reasons as in sequential prediction, though we find the magnitude of this performance reduction to be less extreme in the contemporaneous case.

Table 5 provides a basis for qualitative comparison between our results and related contemporaneous prediction studies that use DHS poverty or malnutrition indicators. Relative to the dirth of such studies for sequential forecasting, we are aware of at least three such papers [7], [12], [9] which apply transfer learning and convolutional neural networks to contemporaneous prediction of DHS asset poverty measures, with the latter also offering a basis for comparison against our malnutrition predictions. Jean *et al.* [7] report out-of-sample, aggregate $r^2 = .59$, with $r^2 \in [0.55, 0.75]$ for individual survey performance across single DHS surveys from five African countries: Malawi, Nigeria, Rwanda, Tanzania and Uganda. Yeh *et al.* [12] report an aggregate $r^2 = .67$, and mean country-level $r^2 = .70$, with predictions done at the village level, using DHS surveys across 23 African countries. Head *et al.* [9] used four surveys, conducted in Honduras, Nepal, Nigeria, and Rwanda, and report survey specific $r^2 \in [0.51, 0.74]$ for asset wealth, $r^2 \in [0.31, 0.47]$ for underweight female BMI, $r^2 \in [0.03, 0.35]$ for child height percentile, and $r^2 \in [-.02, -.11]$ for child height-to-weight percentile.

Again, our random forest models perform comparably to these more sophisticated models. Our aggregate performance in asset poverty prediction is almost to the $r^2 = .59$ reported by Jean *et al.* [7], despite using simpler methods, but is outperformed by Yeh *et al.* [12]. Our models do less well in predicting female underweight BMI than Head *et al.* [9] but as well or better in predicting child nutritional outcomes. A clear, relative weakness of our method is evident when assessing model performance at fine (i.e. survey level) scales, falling on the low end of the performance spectrum and being clearly outdone by by Yeh *et al.* [12], indicating again the relative strength of transfer learning methods which are less reliant on sample size. Again emphasizing the challenges of direct comparison due to differences in the exact encodings of DHS derived outcomes, we again find simple RF methods and open source data can produce competitive results for contemporaneous prediction of poverty and malnutrition in aggregate, with the caveat of underperformance at country or survey specific levels of analysis, relative to state of the art. As in sequential forecasting, we interpret these comparisons as suggesting that relatively straightforward RF models and open source data can provide reasonable first pass estimates of poverty and malnutrition prevalances, which can supplement contemporaneous survey-based estimates for geographic targeting and for monitoring and evaluation purposes, while being considerably easier for agencies to adopt than competing methods.

Table 5. Summary comparison to related works for contemporaneous prediction of DHS derived malnutrition and poverty indicators.

Paper	Child Stunting	Child Wasting	Asset Poverty	Underwt Women
Jean *et al.* [7]			0.59, 0.55-0.75†	
Head *et al.* [9]	0.03-0.35†	-0.02-0.11†	0.51-0.74†	0.31-0.47†
Yeh *et al.* [12]			0.67, 0.70*	
Us	0.28, 0.21*, 0.17†	0.23, 0.09*, 0.08*	0.58 , 0.49*, 0.44†	0.48 , 0.24*, 0.20†

Unmarked, $\star$, and $\dagger$ flagged r^2 values represent aggregate, mean country, and mean survey level, results respectively. Note that Head *et al.* [9] reports predictive performance for child weight for height percentage and child height percentile, which are not directly comparable to our wasting or stunting metrics, and we estimate their performance on the latter from a figure.

4.3 Feature importance

Understanding what features are most informative of poverty and malnutrition status can help inform aid programs and prioritize future data collection efforts. We provide here a brief summary of feature variable importance. Feature importances are reported as the mean decrease in impurity (MDI) for each feature, which loosely measures the extent to which inclusion of a given feature improves the fit of our MRF model. Given a feature x, decrease in impurity is calculated as the product of the percentage of training samples split on x, times the resulting decrease in model cost (variance) resulting from such splits, with MDI defined as the average of these quantities across the forest ensemble. MDI is reported separately for both our sequential and contemporaneous frameworks, with Figs 4 and 5 displaying the average MDI for each feature across all surveys (i.e. in aggregate), and across all surveys within each country, respectively.

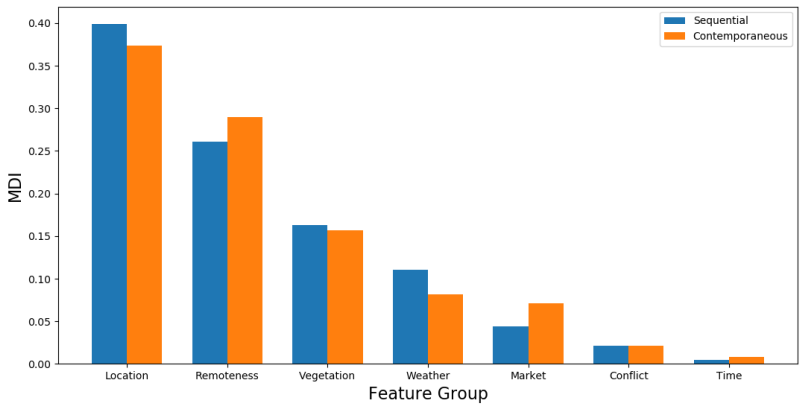

Fig 4. Mean MDI over all surveys, grouped by data source. Location refers to survey latitude, longitude, altitude, and slope. Remoteness indicates urban-rural status and distance to nearest major city. Vegetation includes pasture coverage, tree coverage, and SIF readings. Weather includes CHRPS and LST data. Market contains all food price data.

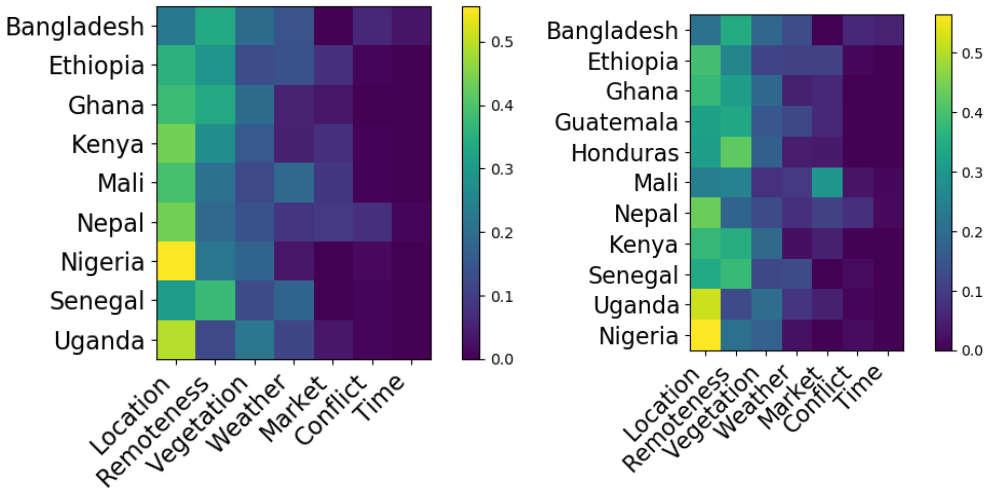

(a) Sequential **(b)** Contemporaneous

Fig 5. Mean relative variable importance across survey years, indexed by country and data source.

Fig 4 shows that physical geography features indicating EA location and remoteness account for the largest share of predictive skill in both contemporaneous and sequential models. While effective for prediction and a confirmation of the value of geographic targeting, these relationships are clearly non-causal and relatively static, and thus somewhat dissatisfying from a policy and planning perspective. We also note, however, that both vegetation and weather features meaningfully contribute to skill in predicting poverty and malnutrition, particularly in the sequential forecasting framework that is appropriate to early warning systems.

Perhaps surprisingly, given the considerable attention paid to conflict and food price shocks as drivers of poverty and malnutrition, those features exhibit comparatively little predictive power. This may be partially an artifact of our data construction and cleaning process. Inter-country variation in food price data availability led us to exclude features missing for more than 20 percent of periods within a given test-train framework in preprocessing, which mechanically reduced the overall importance of these features in aggregate, implying that enhanced focus on market price data collection might still prove useful to poverty and malnutrition estimation. The relative unimportance of time as a predictive feature within our random forest model is unsurprising. Given that our testing points are always drawn from a single survey year, only one branch of any tree split on time will be followed during testing, with the split itself simply acting to discard older data.

5 Conclusion

As they grapple with the broad consequences of the global pandemic and resulting economic disruptions, governments, development and humanitarian organizations worldwide need more than ever practical forecasting tools to target beneficiaries, monitor and evaluate interventions, and or provide early warning of prospective increases in malnutrition or poverty prevalence. Furthermore, given limited financial and human resources, there seems widespread preference for tools that can rely just on free, open access, RS data and relatively simple statistical methods. In this paper, we

demonstrate the viability of both contemporaneous and sequential prediction of malnutrition and poverty prevalence using a set of features drawn from open access data sources and relatively simple random forest methods. The modest success of our independent and Mahalanobis multivariate random forest models signals that simple methods and free, publicly available data can generate predictions of poverty and malnutrition prevalence that are tolerably accurate, and produce models comparable in accuracy to past published studies that rely on more sophisticated deep or transfer learning based methods, proprietary data, or both. Moreover, as data availability continues to grow, the advantage that deep or transfer learning methods have in overcoming sparse data problems will attenuate further.

We find that multivariate, joint prediction of multiple malnutrition and poverty indicators modestly improves predictive performance for some prevalences in sequential prediction, but not in contemporaneous prediction. Given the simplicity of our joint modeling, this finding may indicate that more nuanced joint prediction of poverty and malnutrition status may offer a promising direction of future work, which until now has been overlooked in the literature. We note as well that physical geography features contribute the most to predictive performance, underscoring the value of geographic targeting and the importance of good spatial data. Weather and vegetation data are relatively more important for sequential prediction associated with early warning tasks than with contemporaneous prediction. Overall, predictive errors reflected in normalized root mean squared errors average just 10-25 percent of the range of the target prevalence rate of interest in both contemporaneous and sequential estimation for each of the five malnutrition and poverty indicators we study, signalling that big data and machine learning methods have real potential to inform development and humanitarian programming as these data and methods become more widely available.

5.1 Acknowledgements

We thank Kathy Baylis, Marshall Burke, Stefano Ermon, Nathan Jensen, Erin Lentz, David Lobell, and Rob Vos for helpful discussions, Derek Headey, Soonho Kim and Wahid Quabili for making available curated data series from the Advancing Research on Nutrition and Agriculture (ARENA) Project and the Food Security Portal Project at the International Food Policy Research Institute (IFPRI), Molly Ingram for research assistance, and USAID. These contents are solely the authors' responsibility and do not necessarily reflect the views of USAID or the United States Government.

References

1. Carter MR, Barrett CB. The economics of poverty traps and persistent poverty: An asset-based approach. The Journal of Development Studies. 2006;42(2):178–199.
2. Barrett CB, Carter MR, Chavas JP. The economics of poverty traps. University of Chicago Press Chicago and National Bureau for Economic Research; 2019.
3. Knippenberg E, Jensen N, Constas M. Quantifying household resilience with high frequency data: Temporal dynamics and methodological options. World Development. 2019;121:1–15.
4. Elbers C, Lanjouw JO, Lanjouw P. Micro-level estimation of poverty and inequality. Econometrica. 2003;71(1):355–364.
5. Lang C, Barrett CB, Naschold F. Targeting maps: An asset-based approach to geographic targeting. World development. 2013;41:232–244.
6. Christiaensen L, Lanjouw P, Luoto J, Stifel D. Small area estimation-based prediction methods to track poverty: validation and applications. The Journal of Economic Inequality. 2012;10(2):267–297.
7. Jean N, Burke M, Xie M, Davis WM, Lobell DB, Ermon S. Combining satellite imagery and machine learning to predict poverty. Science. 2016;353(6301):790–794.
8. Ayush K, Uzkent B, Burke M, Lobell D, Ermon S. Generating Interpretable Poverty Maps using Object Detection in Satellite Images. arXiv preprint arXiv:200201612. 2020;.
9. Head A, Manguin M, Tran N, Blumenstock JE. Can human development be measured with satellite imagery? In: ICTD; 2017. p. 8–1.
10. Pokhriyal N, Jacques DC. Combining disparate data sources for improved poverty prediction and mapping. Proceedings of the National Academy of Sciences. 2017;114(46):E9783–E9792.
11. Lentz E, Michelson H, Baylis K, Zhou Y. A data-driven approach improves food insecurity crisis prediction. World Development. 2019;122:399–409.
12. Yeh C, Perez A, Driscoll A, Azzari G, Tang Z, Lobell D, et al. Using publicly available satellite imagery and deep learning to understand economic well-being in Africa. Nature communications. 2020;11(1):1–11.
13. Steele JE, Sundsøy PR, Pezzulo C, Alegana VA, Bird TJ, Blumenstock J, et al. Mapping poverty using mobile phone and satellite data. Journal of The Royal Society Interface. 2017;14(127):20160690.
14. Engstrom R, Hersh J, Newhouse D. Poverty from space: using high-resolution satellite imagery for estimating economic well-being. The World Bank; 2017.
15. Hersh J, Engstrom R, Mann M. Open data for algorithms: mapping poverty in Belize using open satellite derived features and machine learning. Information Technology for Development. 2020;p. 1–30.
16. Masaki T, Newhouse D, Silwal AR, Bedada A, Engstrom R. Small Area Estimation of Non-Monetary Poverty with Geospatial Data. The World Bank; 2020.

17. Bennett CJ, Mitra S. Multidimensional poverty: Measurement, estimation, and inference. Econometric Reviews. 2013;32(1):57–83.

18. Brown ME. Famine early warning systems and remote sensing data. Springer Science & Business Media; 2008.

19. Maxwell D, Khalif A, Hailey P, Checchi F. Determining famine: Multi-dimensional analysis for the twenty-first century. Food Policy. 2020;p. 101832.

20. Mude AG, Barrett CB, McPeak JG, Kaitho R, Kristjanson P. Empirical forecasting of slow-onset disasters for improved emergency response: An application to Kenya's arid north. Food Policy. 2009;34(4):329–339.

21. Tang B, Sun Y, Liu Y, Matteson DS. Dynamic Poverty Prediction with Vegetation Index. In: NeurIPS 2018: Workshop on Modeling and Decision-Making in the Spatiotemporal Domain, 32nd Conference on Neural Information Processing Systems; 2018. .

22. Guo Z, Koo J, Wood S. Fertilizer profitability in East Africa: a spatially explicit policy analysis; 2009.

23. Sebastian K. Atlas of African agriculture research and development: Revealing agriculture's place in Africa. Intl Food Policy Res Inst; 2014.

24. Weiss DJ, Nelson A, Gibson H, Temperley W, Peedell S, Lieber A, et al. A global map of travel time to cities to assess inequalities in accessibility in 2015. Nature. 2018;553(7688):333–336.

25. Hansen M, DeFries R, Townshend J, Carroll M, Dimiceli C, Sohlberg R. Global percent tree cover at a spatial resolution of 500 meters: First results of the MODIS vegetation continuous fields algorithm. Earth Interactions. 2003;7(10):1–15.

26. Ramankutty N, Evan AT, Monfreda C, Foley JA. Farming the planet: 1. Geographic distribution of global agricultural lands in the year 2000. Global biogeochemical cycles. 2008;22(1).

27. Ivanic M, Martin W. Implications of higher global food prices for poverty in low[U+2010]income countries. Agricultural Economics. 2008;39(2008):405–416.

28. Porcar-Castell A, Tyystjärvi E, Atherton J, Van Der Tol C, Flexas J, Pfündel EE, et al. Linking chlorophyll a fluorescence to photosynthesis for remote sensing applications: Mechanisms and challenges. Journal of Experimental Botany. 2014;65(15):4065–4095.

29. Frankenberg C, Hasekamp O, O'Dell C, Sanghavi S, Butz A, Worden J. Aerosol information content analysis of multi-angle high spectral resolution measurements and its benefit for high accuracy greenhouse gas retrievals. Atmospheric Measurement Techniques. 2012;5(7):1809–1821.

30. Peng B, Guan K, Zhou W, Jiang C, Frankenberg C, Sun Y, et al. Assessing the benefit of satellite-based Solar-Induced Chlorophyll Fluorescence in crop yield prediction. International Journal of Applied Earth Observation and Geoinformation. 2020;90:102126.

31. Cai Y, Guan K, Lobell D, Potgieter AB, Wang S, Peng J, et al. Integrating satellite and climate data to predict wheat yield in Australia using machine learning approaches. Agricultural and Forest Meteorology. 2019;274:144–159.

32. Gao Y, Wang S, Guan K, Wolanin A, You L, Ju W, et al. The Ability of Sun-Induced Chlorophyll Fluorescence From OCO-2 and MODIS-EVI to Monitor Spatial Variations of Soybean and Maize Yields in the Midwestern USA. Remote Sensing. 2020;12(7):1111.

33. Guanter L, Zhang Y, Jung M, Joiner J, Voigt M, Berry JA, et al. Global and time-resolved monitoring of crop photosynthesis with chlorophyll fluorescence. Proceedings of the National Academy of Sciences. 2014;111(14):E1327–E1333.

34. Joiner J, Guanter L, Lindstrot R, Voigt M, Vasilkov A, Middleton E, et al. Global monitoring of terrestrial chlorophyll fluorescence from moderate spectral resolution near-infrared satellite measurements: Methodology, simulations, and application to GOME-2. Atmospheric Measurement Techniques. 2013;6(2):2803–2823.

35. Sun Y, Frankenberg C, Jung M, Joiner J, Guanter L, Köhler P, et al. Overview of Solar-Induced chlorophyll Fluorescence (SIF) from the Orbiting Carbon Observatory-2: Retrieval, cross-mission comparison, and global monitoring for GPP. Remote Sensing of Environment. 2018;209:808–823.

36. Yu L, Wen J, Chang C, Frankenberg C, Sun Y. High-resolution global contiguous SIF of OCO-2. Geophysical Research Letters. 2019;46(3):1449–1458.

37. Köhler P, Frankenberg C, Magney TS, Guanter L, Joiner J, Landgraf J. Global retrievals of solar-induced chlorophyll fluorescence with TROPOMI: First results and intersensor comparison to OCO-2. Geophysical Research Letters. 2018;45(19):10–456.

38. Wen J, Köhler P, Duveiller G, Parazoo NC, Magney TS, Hooker G, et al. A framework for harmonizing multiple satellite instruments to generate a long-term global high spatial-resolution solar-induced chlorophyll fluorescence (SIF). Remote Sensing of Environment. 2020 mar;239.

39. Köhler P, Guanter L, Joiner J. A linear method for the retrieval of sun-induced chlorophyll fluorescence from GOME-2 and SCIAMACHY data. 2015;.

40. Anderson MC, Zolin CA, Sentelhas PC, Hain CR, Semmens K, Tugrul Yilmaz M, et al. The Evaporative Stress Index as an indicator of agricultural drought in Brazil: An assessment based on crop yield impacts. Remote Sensing of Environment. 2016;174:82–99.

41. Anderson M, Kustas W. Thermal Remote Sensing of Drought and Evapotranspiration. Eos, Transactions American Geophysical Union. 2008;89(26):233. Available from: `http://doi.wiley.com/10.1029/2008EO260001`.

42. Hu L, Brunsell NA. The impact of temporal aggregation of land surface temperature data for surface urban heat island (SUHI) monitoring. Remote Sensing of Environment. 2013 jul;134:162–174. Available from: `https://linkinghub.elsevier.com/retrieve/pii/S0034425713000631`.

43. Teuling AJ, Taylor CM, Meirink JF, Melsen LA, Miralles DG, van Heerwaarden CC, et al. Observational evidence for cloud cover enhancement over western European forests. Nature Communications. 2017 apr;8(1):14065. Available from: http://www.nature.com/articles/ncomms14065.

44. Hu L, Sun Y, Collins G, Fu P. Improved estimates of monthly land surface temperature from MODIS using a diurnal temperature cycle (DTC) model. ISPRS Journal of Photogrammetry and Remote Sensing. 2020 oct;168(March):131–140. Available from: https://doi.org/10.1016/j.isprsjprs.2020.08.007https://linkinghub.elsevier.com/retrieve/pii/S0924271620302161.

45. Göttsche FM, Olesen FS. Modelling of diurnal cycles of brightness temperature extracted from METEOSAT data. Remote Sensing of Environment. 2001 jun;76(3):337–348. Available from: https://linkinghub.elsevier.com/retrieve/pii/S0034425700002145.

46. Duan SBB, Li ZLL, Tang BHH, Wu H, Tang R, Bi Y, et al. Estimation of diurnal cycle of land surface temperature at high temporal and spatial resolution from clear-sky MODIS data. Remote Sensing. 2014 apr;6(4):3247–3262. Available from: http://www.mdpi.com/2072-4292/6/4/3247/.

47. Inamdar AK, French A, Hook S, Vaughan G, Luckett W. Land surface temperature retrieval at high spatial and temporal resolutions over the southwestern United States. Journal of Geophysical Research. 2008 apr;113(D7):D07107. Available from: http://doi.wiley.com/10.1029/2007JD009048.

48. Mildrexler DJ, Zhao M, Cohen WB, Running SW, Song XP, Jones MO. Thermal Anomalies Detect Critical Global Land Surface Changes. Journal of Applied Meteorology and Climatology. 2018;57(2):391–411. Available from: http://journals.ametsoc.org/doi/10.1175/JAMC-D-17-0093.1.

49. Funk CC, Peterson PJ, Landsfeld MF, Pedreros DH, Verdin JP, Rowland JD, et al. A quasi-global precipitation time series for drought monitoring. US Geological Survey data series. 2014;832(4):1–12.

50. Funk C, Peterson P, Landsfeld M, Pedreros D, Verdin J, Shukla S, et al. The climate hazards infrared precipitation with stations—a new environmental record for monitoring extremes. Scientific data. 2015;2(1):1–21.

51. Dinku T, Funk C, Peterson P, Maidment R, Tadesse T, Gadain H, et al. Validation of the CHIRPS satellite rainfall estimates over eastern Africa. Quarterly Journal of the Royal Meteorological Society. 2018;144:292–312.

52. Goshu EL, Upadhyaya S, Ramsankaran R. Meteorological Drought Monitoring Across Different Rainfall Regimes of Ethiopia Using Chirps V2-Rainfall Data. In: 38th Asian Conference on Remote Sensing,(ACRS 2017), New Delhi, India; 2017. .

53. Toté C, Patricio D, Boogaard H, Van der Wijngaart R, Tarnavsky E, Funk C. Evaluation of satellite rainfall estimates for drought and flood monitoring in Mozambique. Remote Sensing. 2015;7(2):1758–1776.

54. Ayehu GT, Tadesse T, Gessesse B, Dinku T. Validation of new satellite rainfall products over the Upper Blue Nile Basin, Ethiopia. 2018;.

55. Usman M, Nichol JE, Ibrahim AT, Buba LF. A spatio-temporal analysis of trends in rainfall from long term satellite rainfall products in the Sudano Sahelian zone of Nigeria. Agricultural and forest meteorology. 2018;260:273–286.

56. Barrett CB. Food security and sociopolitical stability. OUP Oxford; 2013.

57. Pettersson T, Öberg M. Organized violence, 1989–2019. Journal of peace research. 2020;57(4):597–613.

58. Sundberg R, Melander E. Introducing the UCDP georeferenced event dataset. Journal of Peace Research. 2013;50(4):523–532.

59. De'Ath G. Multivariate regression trees: a new technique for modeling species–environment relationships. Ecology. 2002;83(4):1105–1117.

60. Haider S, Rahman R, Ghosh S, Pal R. A copula based approach for design of multivariate random forests for drug sensitivity prediction. PloS one. 2015;10(12).

61. Segal M, Xiao Y. Multivariate random forests. Wiley Interdisciplinary Reviews: Data Mining and Knowledge Discovery. 2011;1(1):80–87.

62. Sahoo K, Sahoo B, Choudhury AK, Sofi NY, Kumar R, Bhadoria AS. Childhood obesity: causes and consequences. Journal of family medicine and primary care. 2015;4(2):187.

63. Oken E, Gillman MW. Fetal origins of obesity. Obesity research. 2003;11(4):496–506.

64. Ploton P, Mortier F, Réjou-Méchain M, Barbier N, Picard N, Rossi V, et al. Spatial validation reveals poor predictive performance of large-scale ecological mapping models. Nature Communications. 2020;11(1):1–11.

65. Walker P. Famine early warning systems: victims and destitution. Routledge; 2013.

66. NET) FEWSNF. Nigeria Food Security Update; June 2013. Available from: https://reliefweb.int/sites/reliefweb.int/files/resources/Nigeria%20Food%20Security%20Update%20June2013.pdf.

S1 Appendix: Predictive results indexed by survey

To examine how the quality of our predictions vary across individual surveys, we provide in Figs S1, S2, S3, S4, S5, full, out-of-sample, r^2 sampling distributions for prediction of DHS prevalence rates at the survey-specific level, for both sequential and contemporaneous prediction and for both independent and Mahalanobis random forests. In Tables S1, S2, S3, S4, we present summary statistics which summarize these results.

	Child Stunting	Child Wasting	Healthy Weight	Asset Poverty	Underwt Women
Mean r^2	0.00	-0.25	-0.38	-0.29	0.09
Median r^2	0.01	-0.03	-0.07	0.14	0.08
Std r^2	0.02	0.14	0.44	2.7	0.03
Mean NRMSE	0.21	0.15	0.16	0.26	0.17
Median NRMSE	0.21	0.16	0.16	0.23	0.18
Std NRMSE	0.00	0.00	0.00	0.01	0.00

Table S1. Summary Statistics for Sequential Prediction with Independent Random Forests with performance measures computed separately for each survey. Mean and standard deviation calculations are weighted by relative survey size.

	Child Stunting	Child Wasting	Healthy Weight	Asset Poverty	Underwt Women
Mean r^2	0.01	-0.05	-0.17	-0.12	0.07
Median r^2	0.00	-0.02	-0.02	0.14	0.05
Std r^2	0.02	0.02	0.10	1.28	0.03
Mean NRMSE	0.21	0.14	0.15	0.26	0.17
Median NRMSE	0.21	0.15	0.16	0.23	0.18
Std NRMSE	0.00	0.00	0.00	0.01	0.00

Table S2. Summary Statistics for Sequential Prediction with Joint Random Forests, with performance measures computed separately for each survey. Mean and standard deviation calculations are weighted by relative survey size.

	Child Stunting	Child Wasting	Healthy Weight	Asset Poverty	Underwt Women
Mean r^2	0.17	0.07	0.04	0.44	0.20
Median r^2	0.09	0.00	0.00	0.46	0.23
Std r^2	0.03	0.02	0.01	0.03	0.02
Mean NRMSE	0.21	0.18	0.19	0.20	0.19
Median NRMSE	0.22	0.20	0.21	0.21	0.19
Std NRMSE	0.00	0.00	0.00	0.00	0.00

Table S3. Summary Statistics for Contemporaneous Prediction with Independent Random Forests with performance measures computed separately for each survey. Mean and standard deviation calculations are weighted by relative survey size.

	Child Stunting	Child Wasting	Healthy Weight	Asset Poverty	Underwt Women
Mean r^2	0.17	0.08	0.04	0.43	0.19
Median r^2	0.09	0.01	0.00	0.45	0.16
Std r^2	0.02	0.02	0.01	0.03	0.02
Mean NRMSE	0.21	0.18	0.19	0.20	0.19
Median NRMSE	0.23	0.20	0.21	0.21	0.19
Std NRMSE	0.00	0.00	0.00	0.00	0.00

Table S4. Summary Statistics for Contemporaneous Prediction with Joint Random Forests, with performance measures computed separately for each survey. Mean and standard deviation calculations are weighted by relative survey size.

.

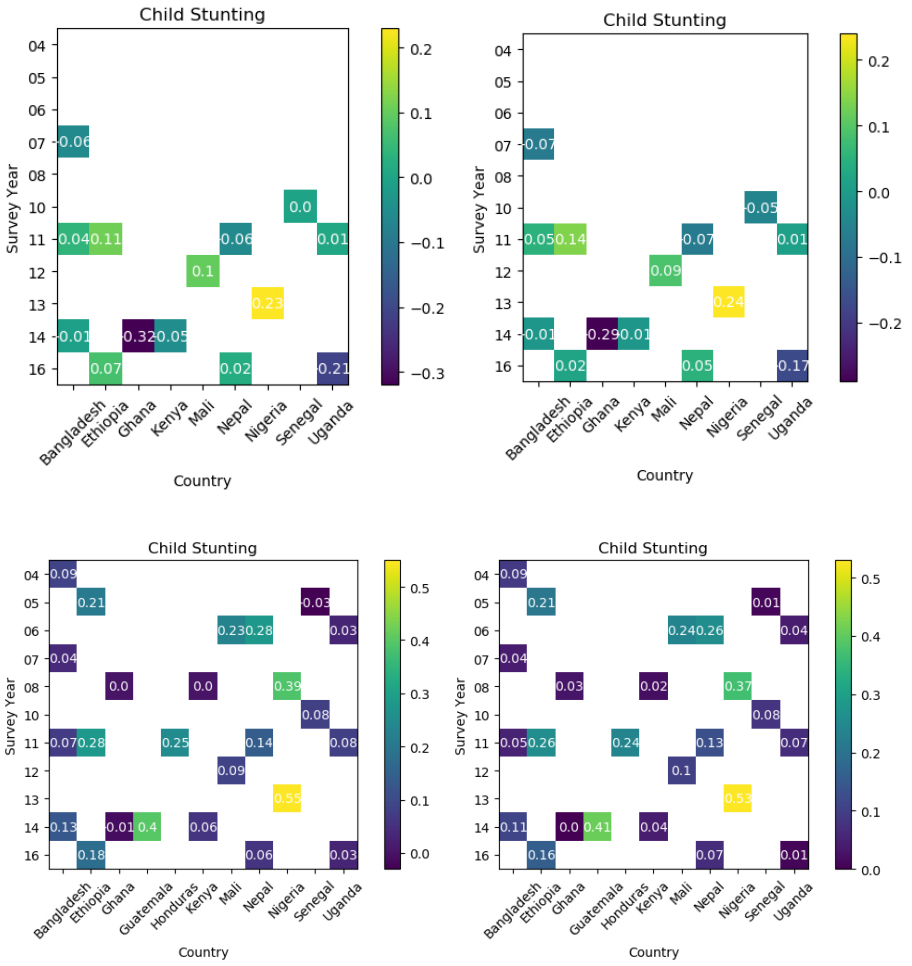

Fig S1. r^2 for Child Stunting prediction, indexed by year, country. Top row: sequential, bottom row: contemporaneous. Left column: Independent RF, Right column: MRF

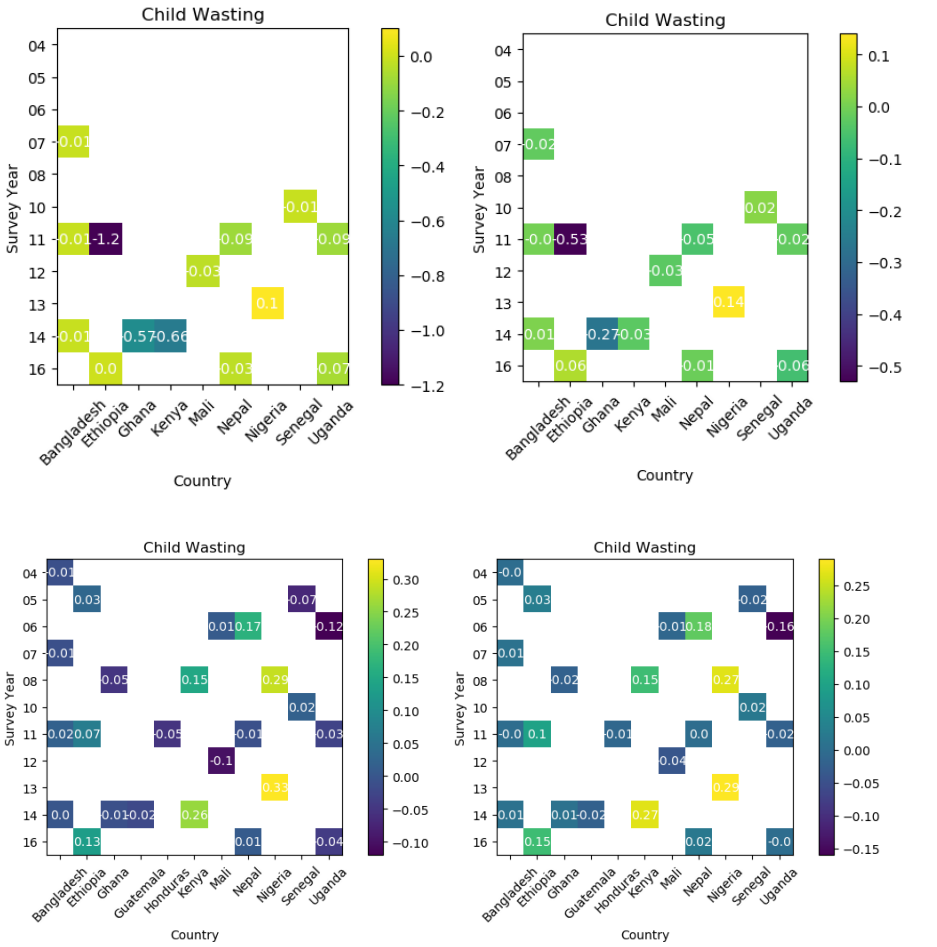

Fig S2. r^2 for Child Wasting prediction, indexed by year, country. Top row: sequential, bottom row: contemporaneous. Left column: Independent RF, Right column: MRF

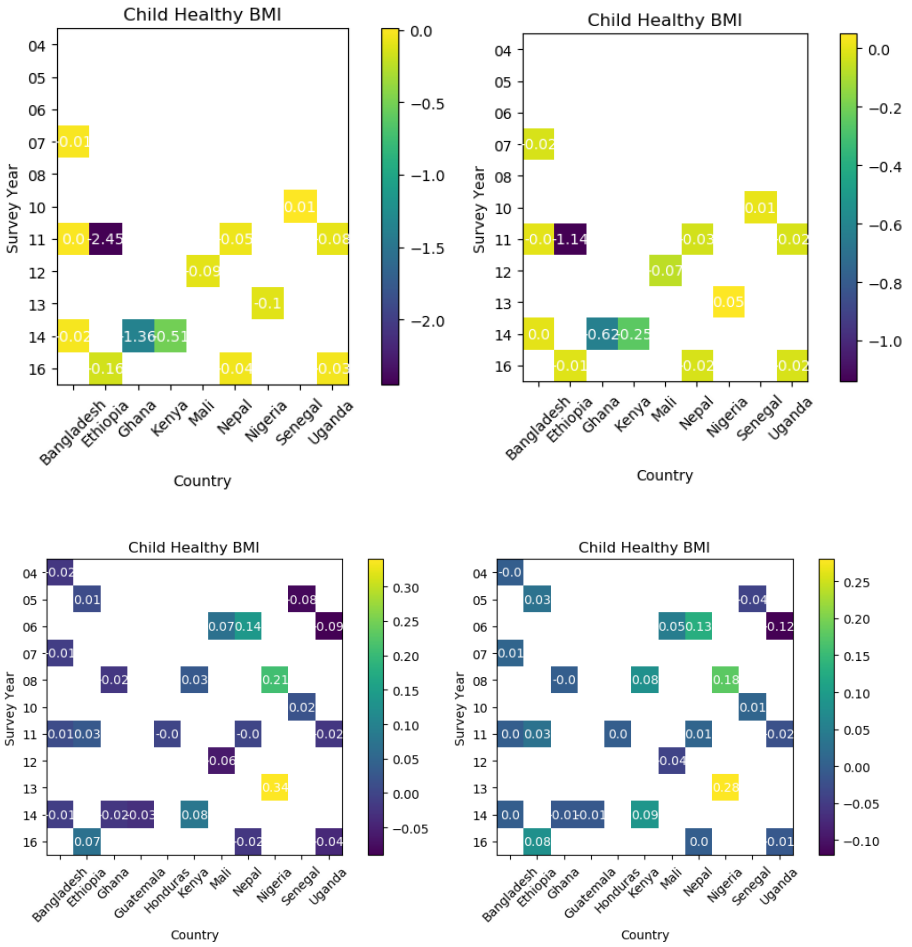

Fig S3. r^2 for Healthy Weight Children prediction, indexed by year, country. Top row: sequential, bottom row: contemporaneous. Left column: Independent RF, Right column: MRF

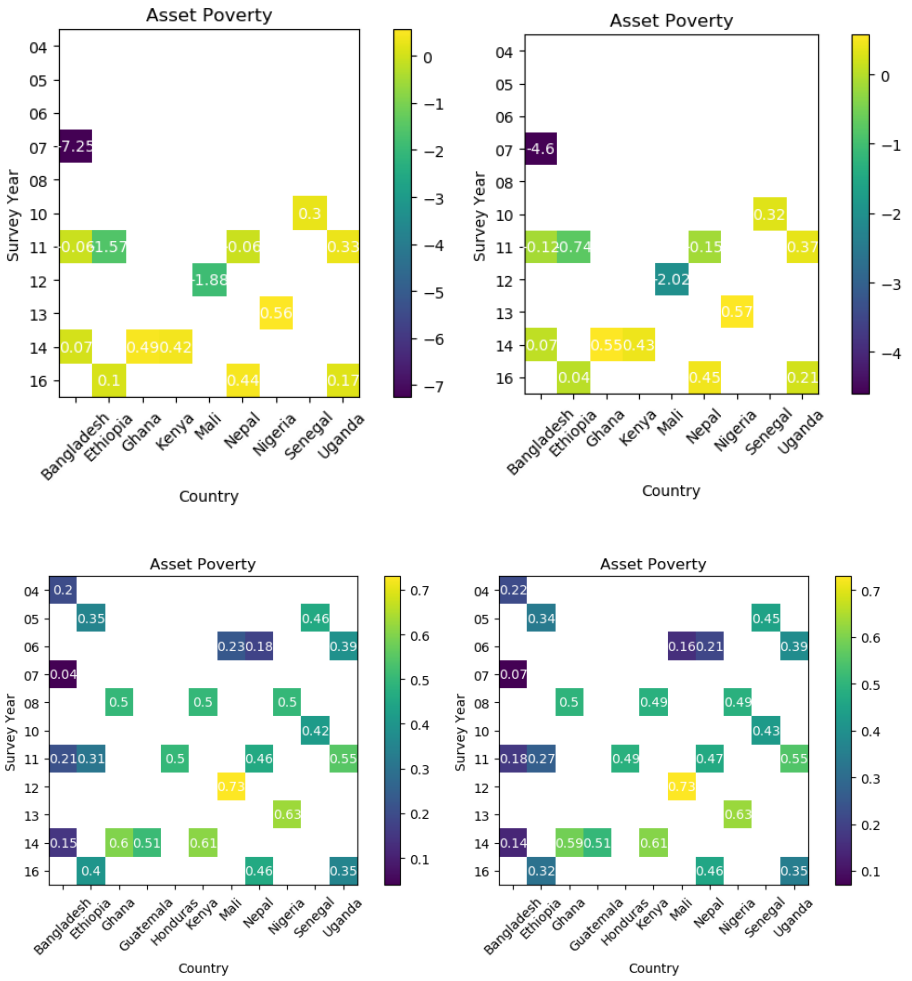

Fig S4. r^2 for Asset Poverty prediction, indexed by year, country. Top row: sequential, bottom row: contemporaneous. Left column: Independent RF, Right column: MRF

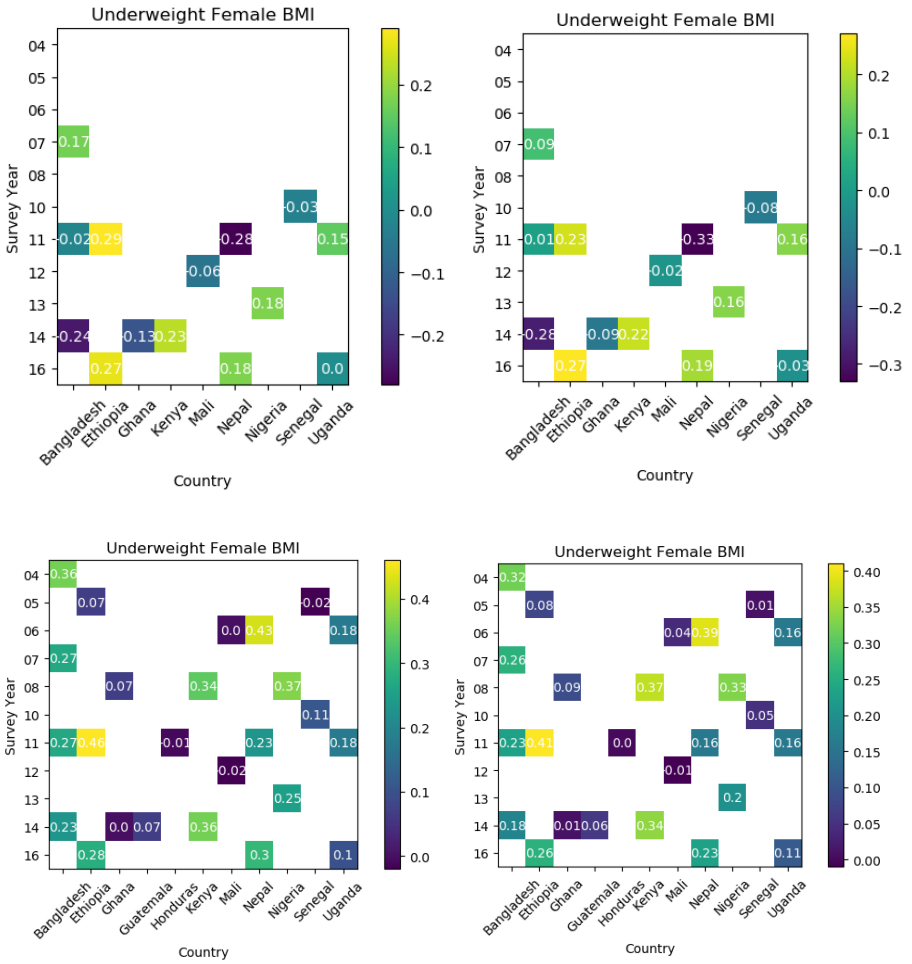

Fig S5. r^2 for Underweight Female BMI prediction, indexed by year, country. Top row: sequential, bottom row: contemporaneous. Left column: Independent RF, Right column: MRF

Relative to our aggregate results shown in Tables 1,3, we immediately notice a significant drop in average r^2 for sequential forecasting of all prevalence rates, alongside a less extreme but still significant decrease in r^2 for contemporaneous prediction, for both joint and independent random forest models. Surprisingly, we find that our NRMSEs stay qualitatively similar to our aggregate results, with errors remaining bound by 10 to 25 percent of an indicators given range, indicating our model can still produce relatively reliable prevalence rate predictions for the purpose of policy informance at survey-level scale, but that these predictions fail to explain the underlying variability in prevalence rates over small spatial domains as a function of input features. This reduction in performance is accompanied by high variability in out-of-sample r^2, and, particularly in the case of sequential forecasting, the emergence of a heavy tail of poor performance. This finding is best emphasized in our forecasting of asset poverty prevalence in Bangladesh 2007, Ethiopia 2011, and Mali 2012 (Fig S4). In contrast, we see surveys with relatively high performance, such as Nigeria, 13. Noting these catastrophic results coincide in all cases with the earliest possible forecast years in relatively small sample size countries, where training and testing sets can be on the order of as few as 300-400 samples (see Table S5 for exact survey sizes),

it seems quite plausible these results are caused by small sample sizes which are insufficient to train random forest models capable of effectively discriminating poverty and malnutrition prevalence. In support of this hypothesis, we display in Fig S6 r^2 and NRMSE as a function of survey size, and note a clear trend moving from small to large scale surveys.

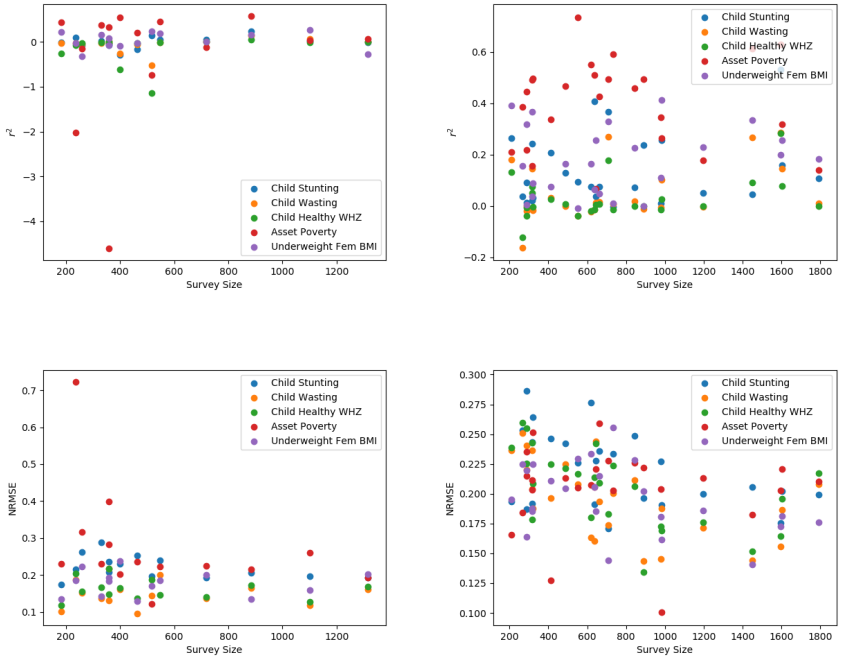

Fig S6. Out-of-sample r^2 and NRMSE for poverty and malnutrition prevalence prediction using MRFs as function of training size. Left Column: Sequential Right: Contemporaneous

While these findings pose a strong motivation for continued collection of poverty and malnutrition surveys to facilitate future remote sensing efforts, it also indicates that the results of our model must be taken with a grain of salt, particularly when performing sequential forecasting on small spatial scales, and indicate a relative strength of transfer learning approaches which are less reliant on sample size. Nevertheless, our positive aggregate results, the existence of some positive results for individual surveys, and generally small NRMSE across these two predictive tasks, seems to indicate our methodology can still be used to generate reasonable first order assessments of poverty and malnutrition prevalence, particularly in countries with higher survey engagement.

S2 Appendix: Supplementary tables

Table S5. Number of DHS enumeration areas used for training and prediction, by country and survey year.

	2004	2005	2006	2007	2008	2010	2011	2012	2013	2014	2016
Bangladesh	361	0	0	361	0	0	600	0	0	600	0
Ethiopia	0	523	0	0	0	0	596	0	0	0	640
Ghana	0	0	0	0	402	0	0	0	0	418	0
Guatemala	0	0	0	0	0	0	0	0	0	802	0
Honduras	0	0	0	0	0	0	1135	0	0	0	0
Kenya	0	0	0	0	397	0	0	0	0	1592	0
Mali	0	0	406	0	0	0	0	407	0	0	0
Nepal	0	0	260	0	0	0	287	0	0	0	370
Nigeria	0	0	0	0	886	0	0	0	895	0	0
Senegal	0	368	0	0	0	388	0	0	0	0	0
Uganda	0	0	363	0	0	0	393	0	0	0	688

Note that although DHS surveys also exist in 2003 for Ghana, Kenya, and Nigeria, these surveys are omitted from our analysis due to inavailability of SIF data for these years. The 2012 and 2014 Senegal DHS surveys are omitted due to missing Underweight Female BMI data.

Table S6. Summary of open access food price data from FAO

Country	No. of food types	No. of markets	Price Type	First available period
Bangladesh	5	1	Retail	7/1998
Ethiopia	5	9	Wholesale	1/2000
Ghana	8	6	Wholesale	1/2006
Guatemala	7	2	Wholesale	1/2000
Honduras	3	3	Wholesale	‘1/2000
Kenya	2	5	Wholesale	1/2006
Mali	4	7	Wholesale	1/2005
Nepal	2	1	Retail	1/2005
Nigeria	6	6	Wholesale	8/2003
Senegal	3	11	Retail	1/2007
Uganda	5	3	Wholesale	1/2006